Electronic Supplementary Information

Curvature-emergent supramolecular polymerization of a porphyrin dyad with a scissor-shaped motif

Ryuichi Kawai,[a] Soichiro Ogi,[b] Hiroki Hanayama,[c] Ryo Kudo,[a] and Shiki Yagai*[c,d]

a. Division of Advanced Science and Engineering, Graduate School of Engineering, Chiba University, 1-33 Yayoi-cho, Inage-ku, Chiba 263-8522, Japan.
b. Intergrated Research Consortium on Chemical Science (IRCCS), Nagoya University Furo, Chikusa, Nagoya 464-8682, Japan.
c. Department of Applied Chemistry and Biotechnology, Graduate School of Engineering, Chiba University, 1-33 Yayoi-cho, Inage-ku, Chiba 263-8522, Japan.
d. Institute for Advanced Academic Research (IAAR), Chiba University, 1-33 Yayoi-cho, Inage-ku, Chiba 263-8522, Japan.

E-mail: yagai@faculty.chiba-u.jp
Fax: +81-(0)43-290-3401
Tel: +81-(0)43-290-3169

Table of Contents

1. Materials and Methods

General

All starting materials and reagents were purchased from commercial suppliers and used without further purification. Medium-pressure column chromatography was carried out with a Biotage Flash Purification System Isolea One using Biotage Sfär Silica HighCapacity Duo 20 μm, 25 g cartridges. Solvents used for the preparation of supramolecular assemblies were of spectral grade and used without further purification. Gel permeation chromatography (GPC) was performed using a recycling preparative liquid chromatography (LC-9225NEXT, Japan Analytical Industry) equipped with two GPC columns (JAIGEL-2HR Plus and JAIGEL-2.5HR Plus). ^{1}H and ^{13}C nuclear magnetic resonance (NMR) spectra were recorded in $CDCl_3$ at 20 °C on a Bruker AVANCE III-400M NMR spectrometer or a Bruker AVANCE III-500M NMR spectrometer. ^{1}H NMR chemical shifts reported in parts per million (ppm, δ) were referenced to the chemical shifts of tetramethylsilane (TMS) at 0.00 ppm. The resonance multiplicity is described as s (singlet), d (doublet), t (triplet), q (quartet), quin (quintet), and m (multiplet). ^{13}C NMR chemical shifts reported in δ (in ppm) were referenced to the chemical shifts of $CDCl_3$ at 77.16 ppm. High-resolution mass spectra (HRMS) were measured on an Exactive (Thermo Fisher Scientific) using electrospray ionization (ESI). Matrix-assisted laser desorption/ionization time-of-flight mass spectrometry (MALDI-TOF-MS) was conducted using a Bruker ultrafleXtreme mass spectrometer. Fourier transform infrared (FT-IR) spectra were measured on a JASCO FT-IR-4600 spectrometer using a 1.0 mm pathlength KBr cell. Dynamic light scattering (DLS) measurements were conducted using Zetasizer Nano (Malvern Instruments) under a 4.0 mW He–Ne laser (λ = 633 nm). Molecular mechanics calculations were carried out using MacroModel (Maestro, version 12.2, Schrödinger) with OPLS2005 force field in the gas-phase. Water concentrations were determined using a Karl Fischer Moisture Titrator (MKC-710, Kyoto Electronics Manufacturing).

Ultraviolet/visible (UV/Vis) absorption spectra

UV/Vis absorption spectra were recorded on a JASCO V-760 spectrophotometer equipped with a JASCO ETCS-761 temperature-control unit. The spectra were recorded using a screw-capped quartz cuvette with a pathlength of 1.0 mm.

Atomic force microscopy (AFM)

AFM images were obtained under ambient conditions using a Multimode 8 Nanoscope V (Bruker AXS) in PeakForce Tapping (ScanAsyst) mode. The scan rate was set to 0.996 Hz. Silicon cantilevers (SCANASYST-AIR) with a spring constant of 0.4 N/m and a resonance frequency of 70 kHz (nominal value, Bruker, Japan) were used. The samples were prepared by spin-coating (3000 rpm, 1 min) approximately 10 μL of MCH solutions of assemblies onto freshly cleaved highly oriented pyrolytic graphite (HOPG, 0.5 cm × 0.5 cm) at room temperature. AFM images were processed using NanoScope Analysis 3.0 (Bruker).

Estimation of the degree of aggregation (α_{agg})

Using the temperature-dependent UV/Vis absorption data, the degree of aggregation (α_{agg}) at a given temperature (T) was calculated from Supplementary Equation S1:

$$\alpha(T)_{agg} = \frac{\varepsilon(T) - \varepsilon_{mon}}{\varepsilon_{agg} - \varepsilon_{mon}} \quad \text{(S1)}$$

where ε_{agg} and ε_{mon} are molar absorption coefficients at 442 nm of fully aggregated (the highest value, α_{agg} = 1) and pure monomeric species (the lowest value, α_{agg} = 0), respectively, and $\varepsilon(T)$ is the molar absorption coefficient at a given temperature.

Isodesmic model fitting

The thermodynamic parameters governing the supramolecular aggregation of **Amo** and **2** were obtained by the global fitting of the melting curves. This global fitting was performed by using the equilibrium model reported by ten Eikelder and co-workers.[S1] The melting curves were obtained by plotting the absorbance at 430 nm or 432 nm against temperature at different total concentrations. The temperature dependence of the equilibrium constant was expressed according to equation S2. From this relationship, the enthalpy change (ΔH) and entropy change (ΔS) were determined. These fits were obtained using MATLAB R2025a.

$$K_{eq}(T) = \exp\left(-\frac{\Delta H - T\Delta S}{RT}\right) \quad \text{(S2)}$$

Cooperative (nucleation-elongation) model fitting

The cooperative assembly process was analyzed using the nucleation-elongation model proposed by Meijer and co-workers.[S2] When the plot of the degree of aggregation (α_{agg}) versus T is non-sigmoidal, the polymerization process can be followed by the cooperative model. In the elongation regimes ($T < T_e$) were fitted with Supplementary Equation S3:

$$\alpha_{agg} = \alpha_{SAT}\left[1 - \exp\left(-\frac{\Delta H_e}{RT_e{}^2}(T - T_e)\right)\right] \quad \text{(S3)}$$

where ΔH_e is the enthalpy release in the elongation regime, α_{SAT} is a parameter the correction coefficient, R is the ideal gas constant, and T_e is the critical temperature.

2. Synthesis and Characterization

Porphyrin derivatives **1** and **2** were synthesized by the following procedure as shown in Scheme S1. The synthesis of **S1**, **S2** and **S3** were reported previously. [S3, S4]

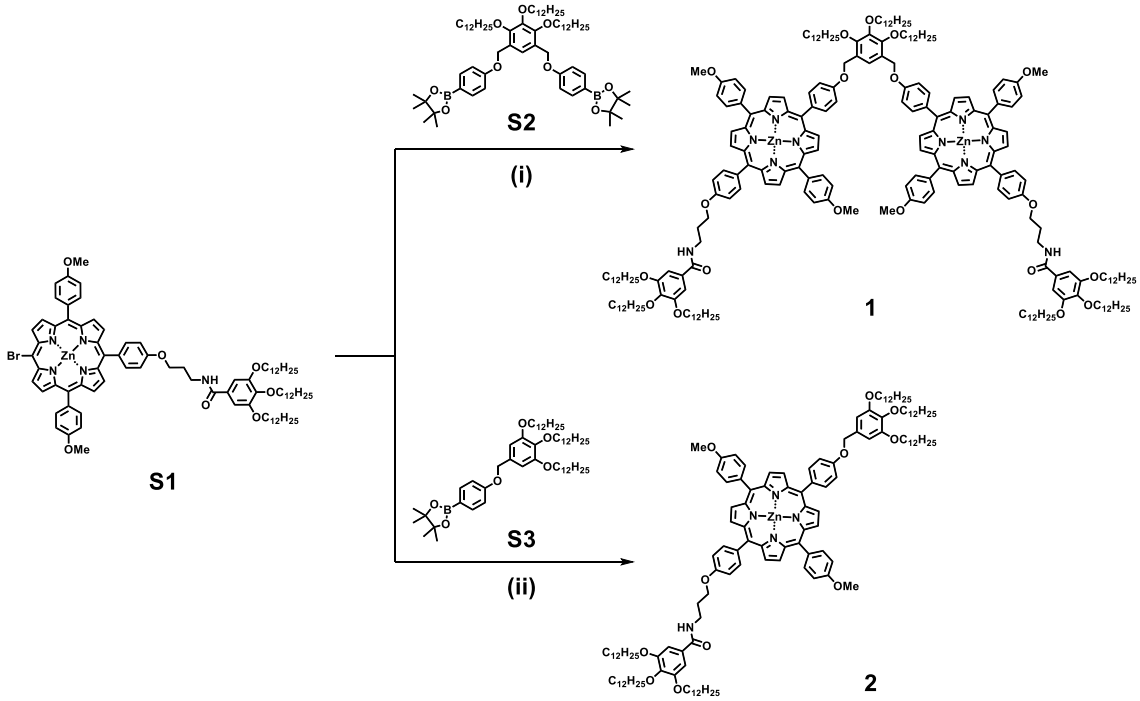

Scheme S1. Synthesis of **1** and **2**. Reagents and conditions: (i) $PdCl_2$(dppf), K_2CO_3, THF:water = 7:1, 70 °C; (ii) $Pd(PPh_3)_4$, K_3PO_4, THF:water = 5:1, 60 °C.

1: Compound **S1** (130 mg, 884 μmol), **S2** (33 mg, 50 μmol), K_2CO_3 (30 mg, 0.22 mmol), and $PdCl_2$(dppf) (10 mg, 12 μmol) were dissolved in a mixture of degassed THF (30 mL) and degassed water (5 mL), and the mixture was stirred for 14 h at 70 °C under an N_2 atmosphere. After cooling to room temperature, the reaction mixture was passed through a small pad of Celite®. The filtrate was diluted with $CHCl_3$ and washed with H_2O and brine. The organic layer was separated, dried over Na_2SO_4, and then evaporated to dryness under reduced pressure. The crude product was purified by column chromatography over silica gel (eluent: $CHCl_3$) and further purified by GPC (eluent: $CHCl_3$) to give **1** as a purple solid (18 mg, 17% yield). ^{1}H NMR (500 MHz, $CDCl_3$, 20 °C, see Chart S1): δ = 9.02–8.91 (m, 16H, β–pyrrole), 8.18 (d, J = 8.4 Hz, 4H, C_6H_4), 8.13 (d, J = 8.5 Hz, 4H, C_6H_4), 8.05 (d, J = 8.6 Hz, 8H, C_6H_4), 7.68 (s, 1H, C_6H), 7.44 (d, J = 8.5 Hz, 4H, C_6H_4), 7.28 (d, J = 8.5 Hz, 4H, C_6H_4), 7.06 (d, J = 8.6 Hz, 8H, C_6H_4), 7.03 (s, 4H, C_6H_2), 6.70 (t, J = 5.5 Hz, 2H, –CON*H*–), 5.43 (s, 4H, C_6HCH_2–O–), 4.42 (t, J = 5.5 Hz, 4H, –CONHCH$_2$CH$_2$CH_2O–), 4.28 (t, J = 6.8 Hz, 4H, –OCH_2CH$_2$CH$_2$(CH$_2$)$_8$CH$_3$), 4.17 (t, J = 6.6 Hz, 2H, –OCH_2CH$_2$CH$_2$(CH$_2$)$_8$CH$_3$), 4.04 (t, J = 6.5 Hz, 8H, –

OC*H*$_2$CH$_2$CH$_2$(CH$_2$)$_8$CH$_3$), 3.98 (t, *J* = 6.8 Hz, 4H, –OC*H*$_2$CH$_2$CH$_2$(CH$_2$)$_8$CH$_3$), 3.84 (s, 12H, –O*Me*), 3.78 (q, *J* = 6.0 Hz, 4H, –CONHC*H*$_2$CH$_2$CH$_2$O–), 2.30 (quin, 4H, –CONHCH$_2$C*H*$_2$CH$_2$O–), 1.92–1.71 (m, 18H, –OCH$_2$C*H*$_2$CH$_2$(CH$_2$)$_8$CH$_3$), 1.59–1.40 (m, 18H, –OCH$_2$CH$_2$C*H*$_2$(CH$_2$)$_8$CH$_3$), 1.26–1.13 (m, 144H, –OCH$_2$CH$_2$CH$_2$(C*H*$_2$)$_8$CH$_3$), 0.89–0.73 (m, 27H, –OCH$_2$CH$_2$CH$_2$(CH$_2$)$_8$C*H*$_3$). ^{13}C NMR (126 MHz, $CDCl_3$, 20 °C, see Chart S2): δ = 167.45, 158.99, 158.71, 158.22, 153.14, 151.95, 150.59, 150.56, 150.47, 150.36, 145.91, 141.25, 135.87, 135.51, 135.47, 135.43, 135.29, 132.00, 131.93, 131.87, 131.71, 129.55, 126.15, 120.89, 120.73, 120.35, 112.94, 112.55, 111.97, 105.72, 74.47, 73.88, 73.52, 69.46, 67.29, 65.62, 55.39, 38.55, 31.96, 31.93, 31.86, 30.61, 30.52, 30.34, 29.77, 29.73, 29.67, 29.61, 29.58, 29.42, 29.38, 29.32, 29.29, 29.19, 26.35, 26.28, 26.10, 22.71, 22.68, 22.64, 22.60, 14.13, 14.08, 14.02. HRMS (MALDI): *m*/*z* calcd for $C_{228}H_{308}N_{10}O_{19}Zn_2$ 3618.206 $[M]^+$, found 3618.115.

2: Compound **S1** (102 mg, 693 μmol), **S3** (60 mg, 0.70 mmol), K_3PO_4 (56 mg, 0.26 mmol), and $Pd(PPh_3)_4$ (8 mg, 7 μmol) were dissolved in a mixture of degassed THF (20 mL) and degassed water (7 mL), and the mixture was stirred for 11 h at 60 °C under an N_2 atmosphere. After cooling to room temperature, the reaction mixture was passed through a small pad of Celite®. The filtrate was diluted with $CHCl_3$ and washed with H_2O and brine. The organic layer was separated, dried over Na_2SO_4, and then evaporated to dryness under reduced pressure. The crude product was purified by column chromatography over silica gel (eluent: EtOAc:*n*-hexane = 1:3) and further purified by GPC (eluent: $CHCl_3$) to give **2** as a purple solid (25 mg, 17% yield). ^{1}H NMR (500 MHz, $CDCl_3$, 20 °C, see Chart S3): δ = 8.97–8.94 (m, 8H, β-pyrrole), 8.14–8.12 (m, 8H, C$_6$*H*$_4$), 7.36 (d, *J* = 8.6 Hz, 2H, C$_6$*H*$_4$), 7.29–7.26 (m, 6H, C$_6$*H*$_4$), 6.93 (s, 2H, C$_6$*H*$_2$), 6.81 (s, 2H, C$_6$*H*$_2$), 6.62 (t, *J* = 5.7 Hz, 1H, –CON*H*–), 5.23 (s, 2H, C$_6$HC*H*$_2$–O–), 4.39 (t, *J* = 5.4 Hz, 4H, –CONHCH$_2$CH$_2$C*H*$_2$O–), 4.10 (s, 6H, –O*Me*), 4.09–3.96 (m, 12H, –OC*H*$_2$CH$_2$(CH$_2$)$_9$CH$_3$), 3.67 (q, *J* = 5.8 Hz, 4H, –CONHC*H*$_2$CH$_2$CH$_2$O–), 2.24 (quin, 2H, –CONHCH$_2$C*H*$_2$CH$_2$O–), 1.89–1.69 (m, 12H, –OCH$_2$C*H*$_2$(CH$_2$)$_9$CH$_3$), 1.50–1.12 (m, 108H, –OCH$_2$CH$_2$(C*H*$_2$)$_9$CH$_3$), 0.90–0.81 (m, 18H, –OCH$_2$CH$_2$(CH$_2$)$_9$C*H*$_3$). ^{13}C NMR (126 MHz, $CDCl_3$, 20 °C, see Chart S4): δ = 167.39, 159.24, 158.52, 158.22, 153.43, 153.09, 150.54, 150.50, 150.40, 141.22, 138.18, 135.85, 135.63, 135.50, 135.45, 135.40, 135.30, 131.90, 131.76, 129.40, 120.77, 120.72, 120.40, 112.94, 112.55, 112.06, 106.53, 105.64, 73.51, 70.83, 69.44, 69.27, 67.28, 55.55, 38.47, 31.97, 31.93, 31.86, 30.42, 30.34, 29.80, 29.73, 29.70, 29.68, 29.61, 29.57, 29.49, 29.42, 29.38, 29.28, 29.12, 26.20, 26.18, 26.10, 22.72, 22.70, 22.68, 22.64, 14.12, 14.10, 14.08. HRMS (ESI): *m*/*z* calcd for $C_{135}H_{193}N_5O_{11}ZnNa$ 2147.3880 $[M+Na]^+$, found 2147.3845.

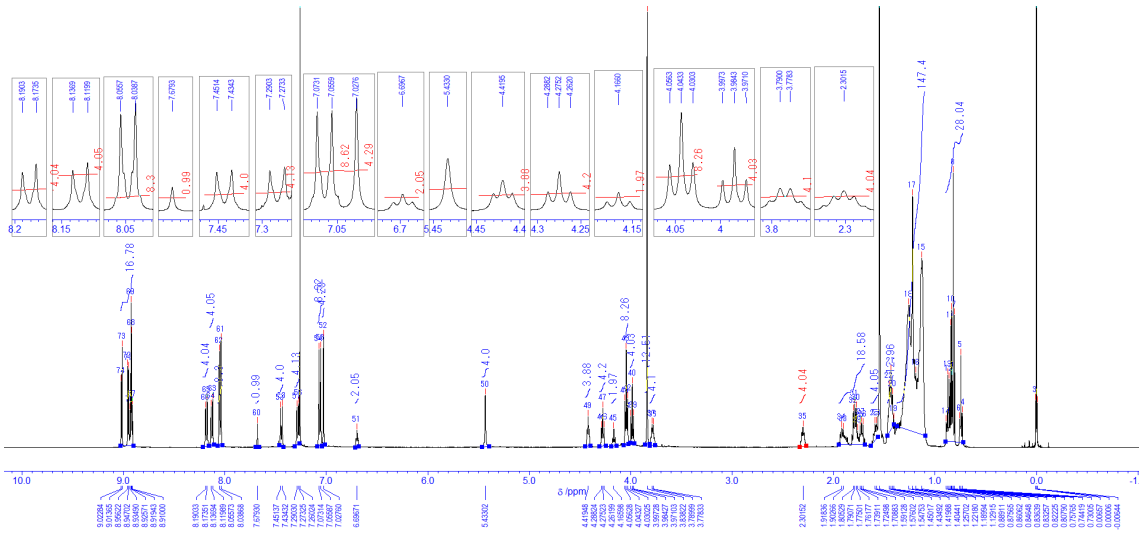

Chart S1. ^{1}H NMR spectrum of **1**.

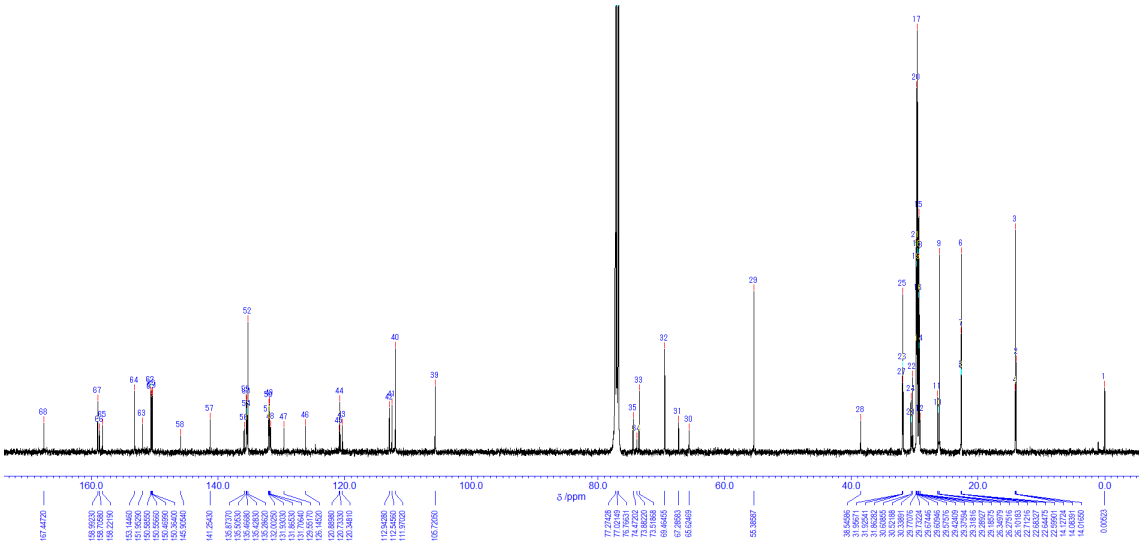

Chart S2. ^{13}C NMR spectrum of **1**.

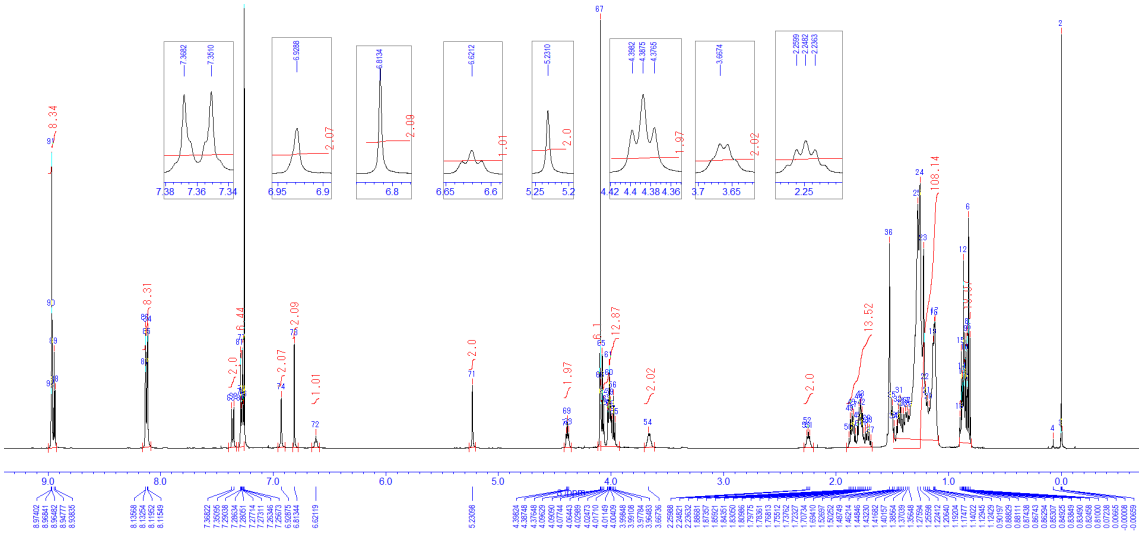

Chart S3. ^{1}H NMR spectrum of **2**.

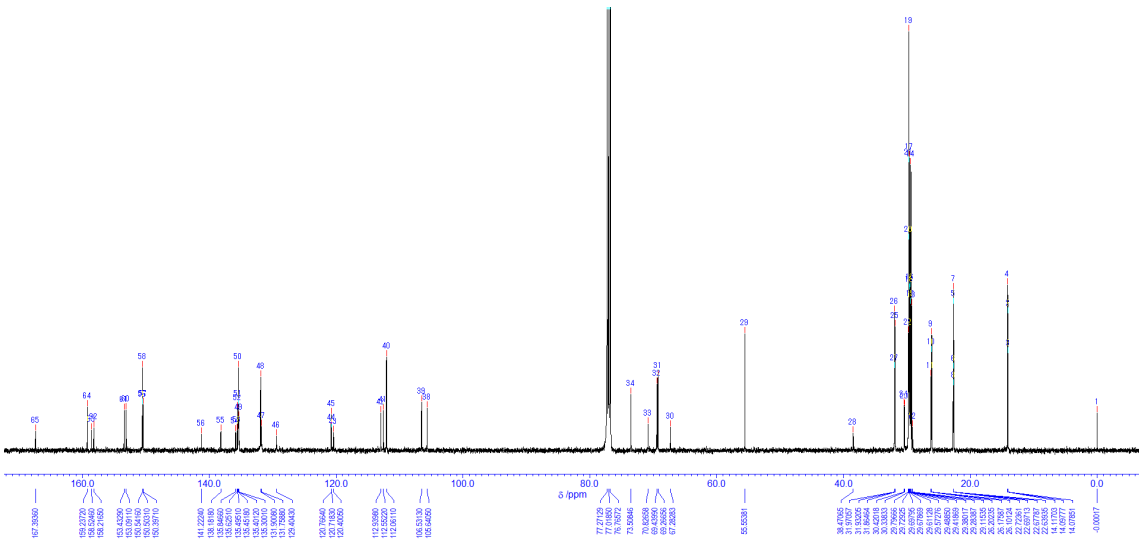

Chart S4. ^{13}C NMR spectrum of **2**.

3. Supporting Figures

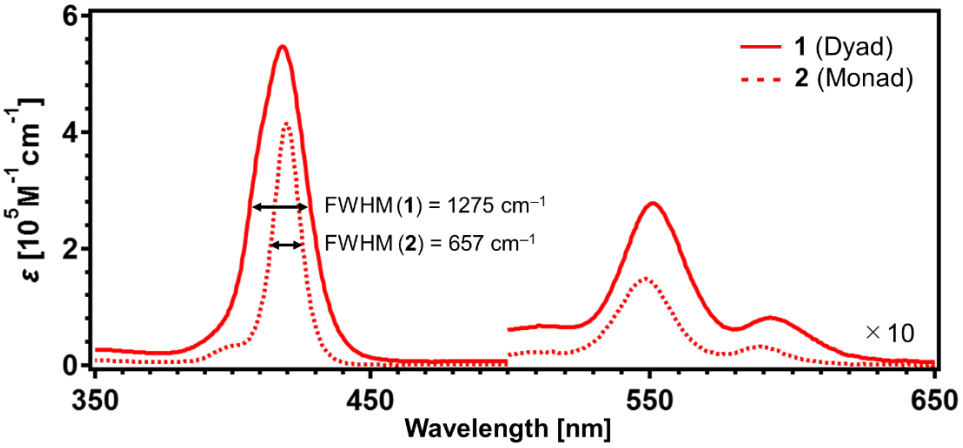

Figure S1. UV/Vis absorption spectra of porphyrin dyad **1** (c = 50 μM, dashed line) and reference monad **2**[S3] (c = 100 μM, solid line) in MCH at 100 °C.

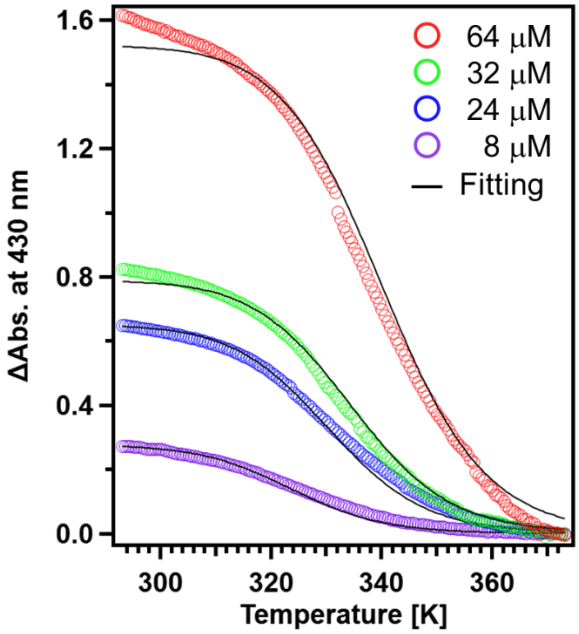

Figure S2. Heating curves of **Amo** of **1** (c = 64, 32, 24, and 8 × 10^{-6} M) recorded by monitoring the absorbance at 430 nm in MCH as a function of temperature. The black represents fits obtained using the isodesmic model in a global fitting approach.[S1]

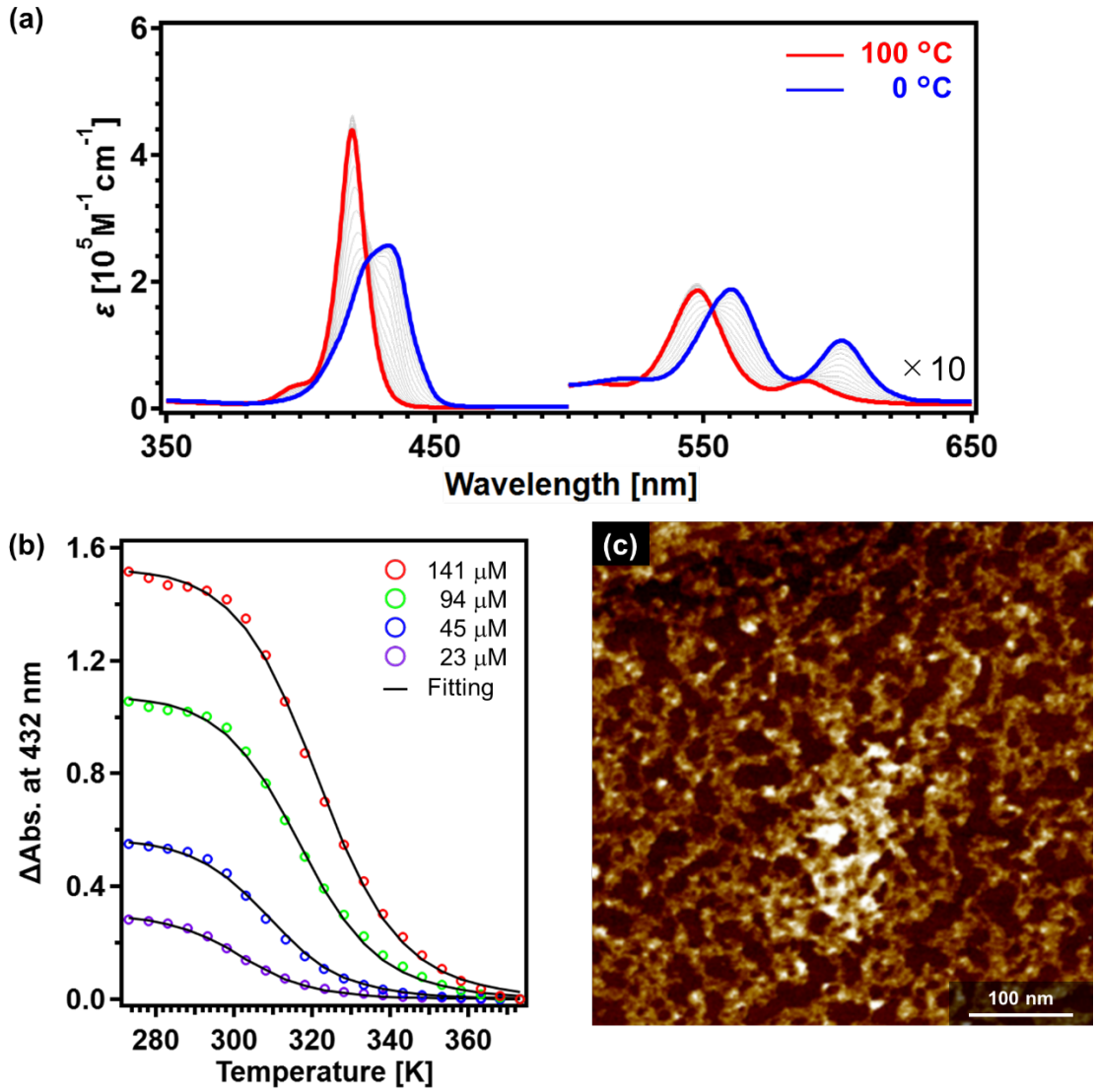

Figure S3. (a) UV/Vis absorption spectra of **2** in MCH (c = 100 µM) upon cooling from 100 °C (red line) to 0 °C (blue line) at a rate of 1 °C min^{-1}. The intermediate spectra were measured every 5 °C. (b) Heating curves of **2** (c = 141, 94, 45, and 23 × 10^{-6} M) recorded by monitoring the absorbance at 432 nm in MCH as a function of temperature. The black represents fits obtained using the isodesmic model in a global fitting approach.[S1] The analysis provided the standard enthalpy ($\Delta H°$) and entropy ($\Delta S°$) of −75.6 kJ mol^{-1} and –162 J mol^{-1} K^{-1}, respectively. (c) AFM image of a MCH solution of **2** prepared by spin-coating immediately after cooling from 100 °C to 0 °C at a rate of 1 °C min^{-1}. AFM imaging of the assemblies of **2** displayed only ill-defined amorphous structures.

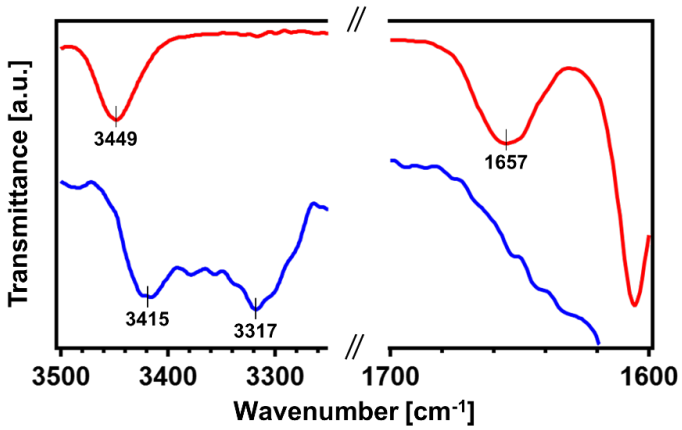

Figure S4. FT-IR spectra of **1** in $CHCl_3$ (c = 300 μM, red line) and MCH (c = 600 μM, blue line). The MCH solution was prepeared by cooling a dilute MCH solution (c = 300 μM), followed by concentration.

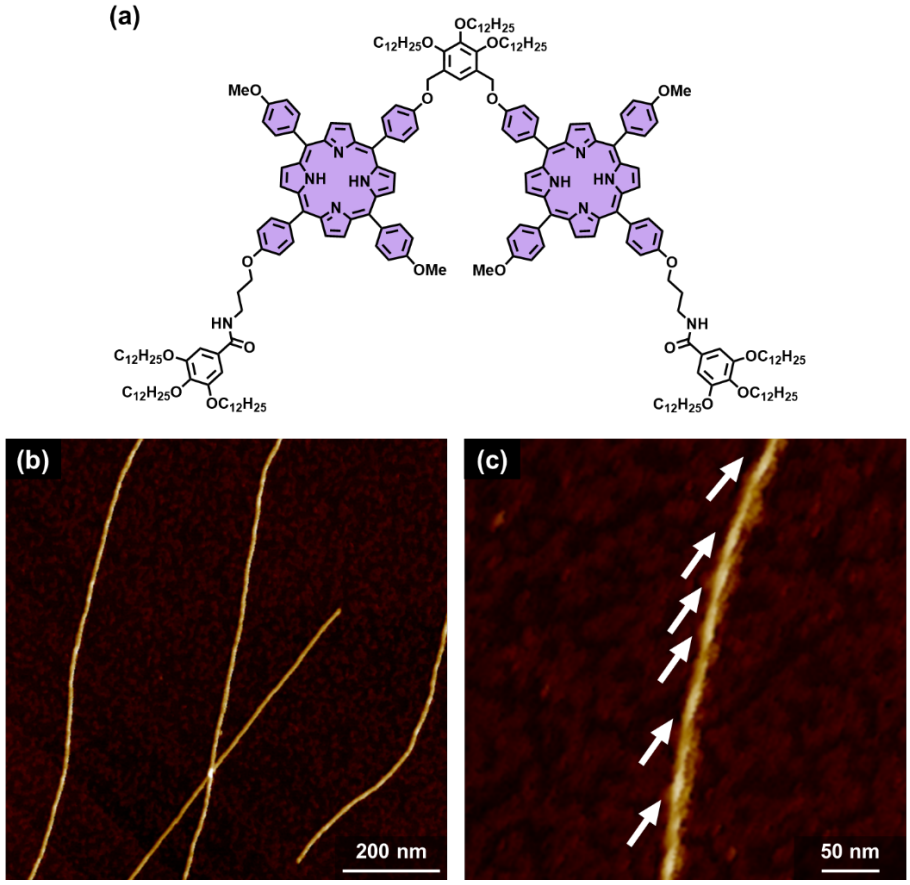

Figure S5. (a) Chemical structure of the previously reported free-base porphyrin dyad.[S3] (b, c) AFM images of helically twisted fibers of in MCH (c = 100 μM).

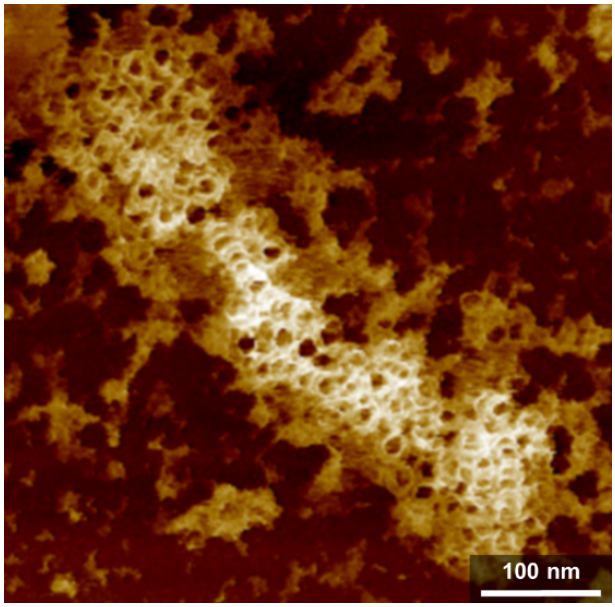

Figure S6. AFM image of $\mathbf{SP_{hel}}$ spin-coated after aging **1** (c = 50 μM) in MCH containing 20% (v/v) toluene for 20 days.

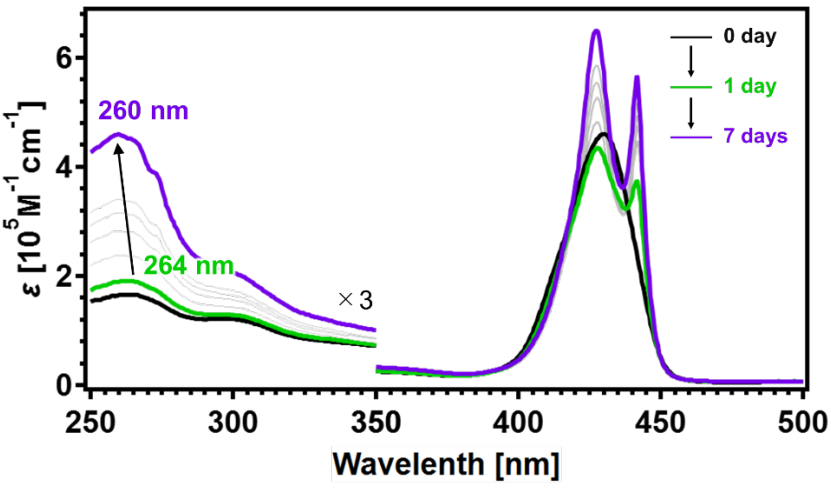

Figure S7. UV/Vis absorption spectra of **1** (c = 50 μM) in MCH aged from 0 day (black line) to 1 day (green line) and 7 days (purple line), respectively.

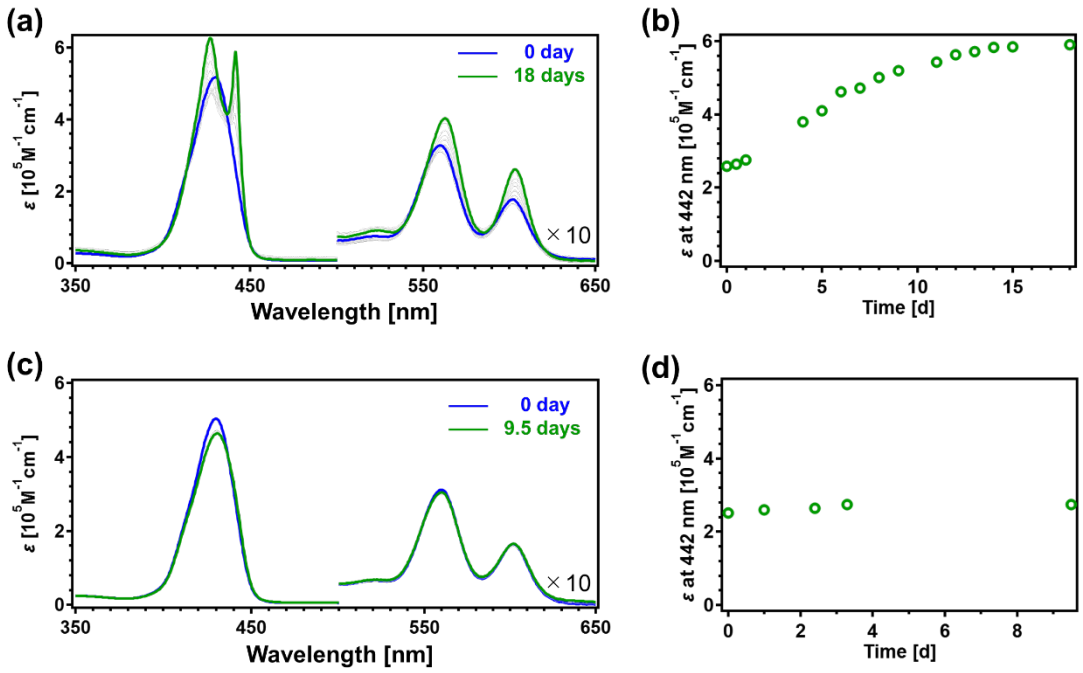

Figure S8. (a, c) UV/Vis absorption spectra of **1** (c = 50 μM) in (a) MCH containing 76 eq. of H_2O aged for 0 day (blue lines) and 18 days (green lines) and in (c) MCH containing 5 eq. of H_2O aged for 0 day (blue lines) and 9.5 days (green lines). Time-dependent changes in the molar extinction coefficient (ε) at 442 nm of **1** in (a) and (d), respectively.

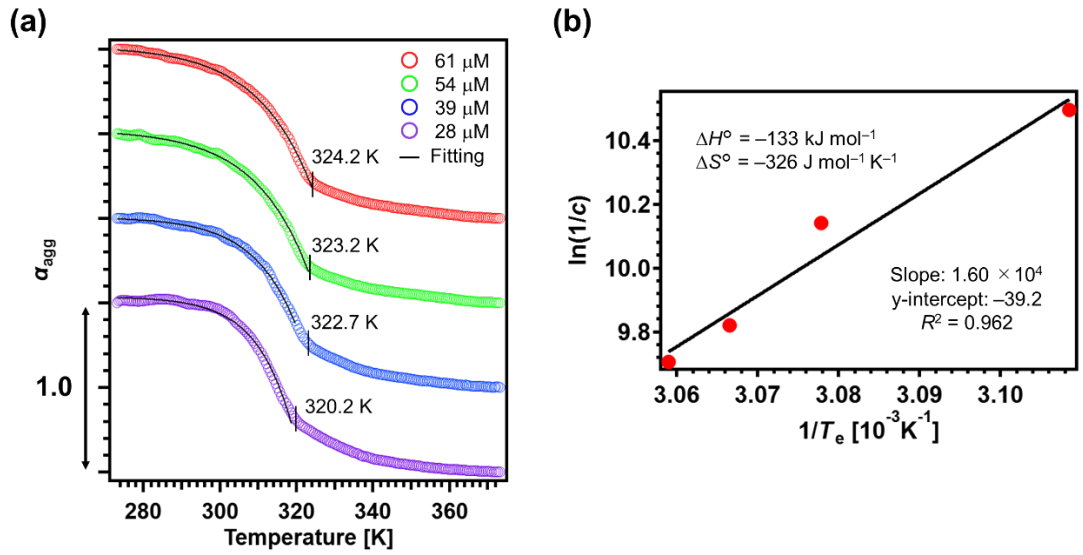

Figure S9. (a) Heating curves of $\mathbf{SP_{hel}}$ of **1** (c = 61, 54, 39, and 28 × 10^{-6} M), obtained by plotting α_{agg} (estimated from the absorption changes at 442 nm) as a function of temperature in MCH containing THF (0.85, 0.70, 0.57 and 0.40 v/v% for c = 61, 54, 39, and 28 × 10^{-6} M, respectively). The black curves show fittings using the cooperative elongation model. (b) van't Hoff analysis of the data in panel (a), obtained by plotting the natural logarithm of the monomer concentrations as a function of T_e^{-1}. The T_e values were determined by the cooperative elongation model fits. For the van't Hoff plots, the monomer concentration at the onset temperature was assumed to be equal to the total monomer concentration. The black line indicates the linear fit.

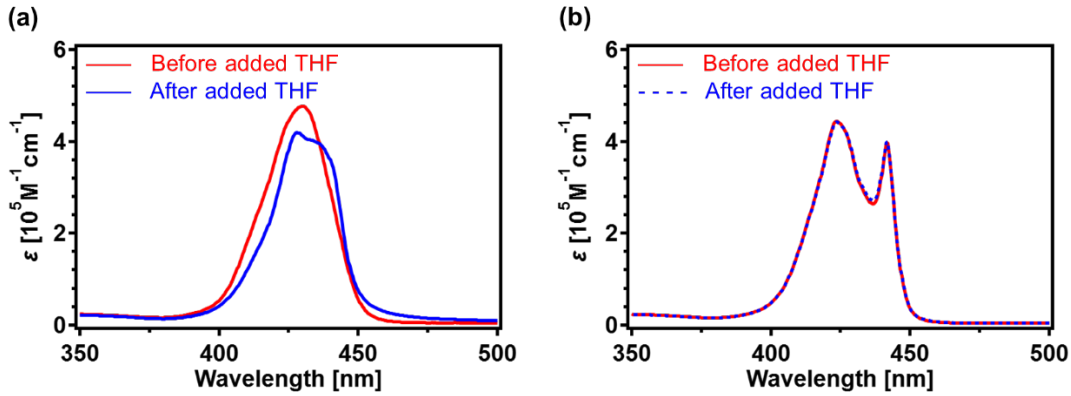

Figure S10. (a, b) UV/Vis absorption spectra of (a) **Amo** solutions of **1** (c = 50 μM) in MCH, showing the spectra before (red) and after adding 1760 eq. of THF, followed by aging for 20 min (blue), and (b) $\mathbf{SP_{hel}}$ solutions of **1** (c = 50 μM) in MCH including 0.7% (v/v, 1760 eq.) THF, showing the spectra before (red) and after adding 1760 eq. THF, followed by aging for 30 min (blue).

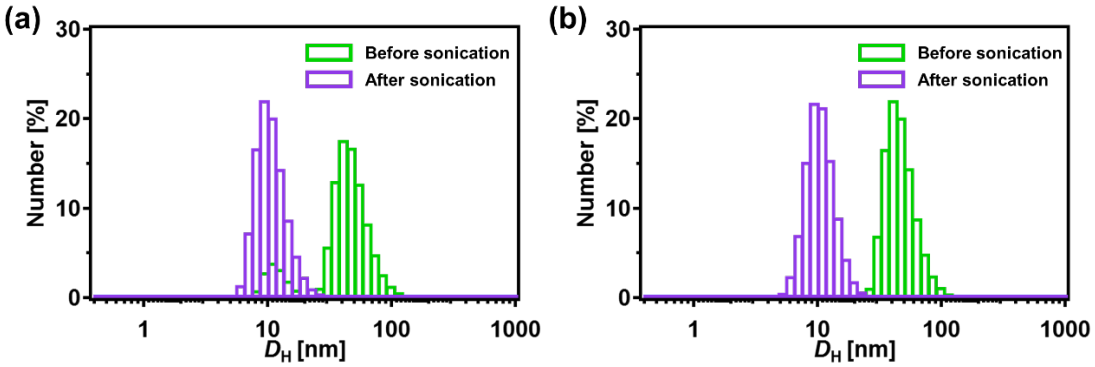

Figure S11. (a, b) DLS size distribution of **1** (c = 50 μM) in (a) MCH and (b) MCH containing 0.7% (v/v) THF, recorded before (green bars) and after (purple bars) sonication.

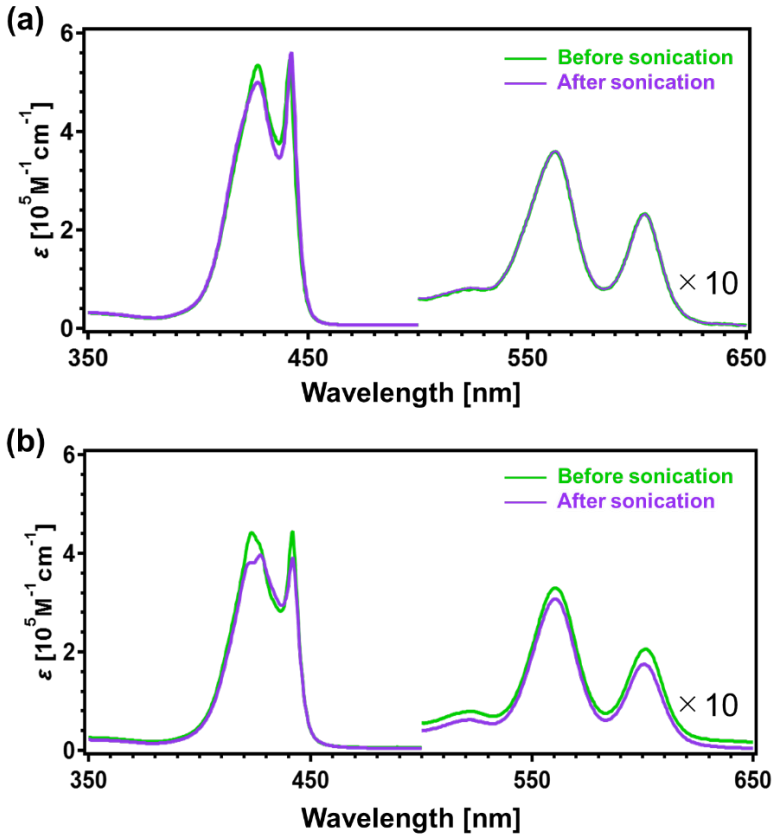

Figure S12. (a, b) UV/Vis absorption spectra of $\mathbf{SP}_{\mathbf{ring}}$ solutions of **1** (c = 50 μM) in (a) MCH and (b) MCH containing THF (c = 50 μM), showing the spectra before (green) and after sonication (purple).

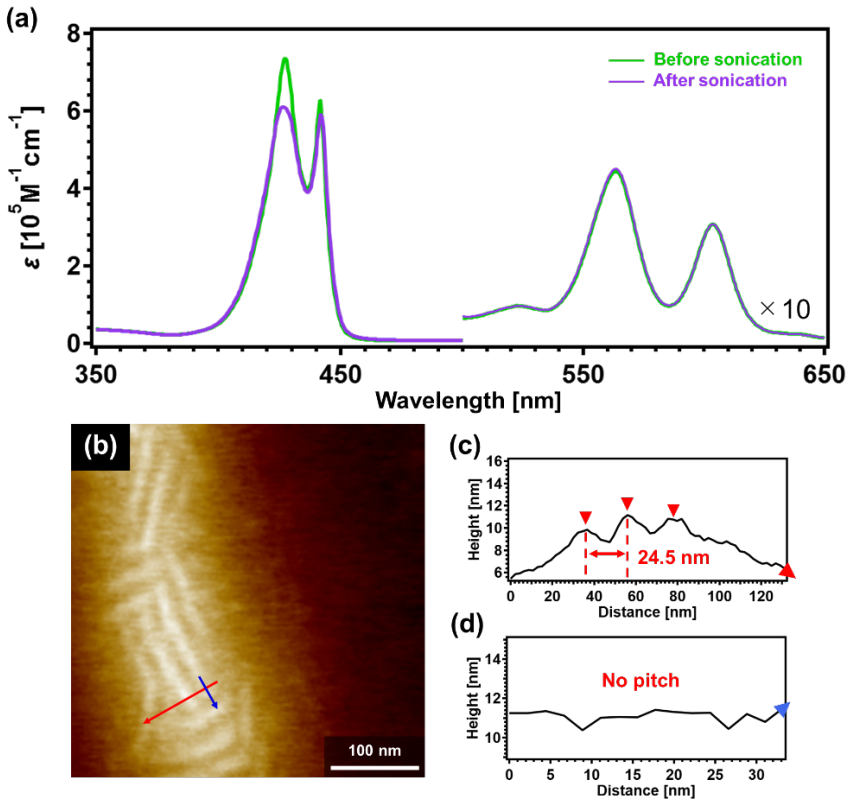

Figure S13. (a) UV/Vis absorption spectra of the 7-day-aged MCH solution of **1** (c = 50 μM) before (green line) and after sonication (purple line). (b) AFM image of the 7-day aged aggregates after sonication. (c, d) AFM cross-sectional analysis along the (c) red and (d) blue arrows in (b).

4. Supporting reference

S1. H. M. M. ten Eikelder, A. J. Markvoort, T. F. A. de Greef, and P. A. J. Hilbers, *J. Phys. Chem. B.,* 2012, **116**, 5291–5301.

S2. P. Jonkheijm, P. van der Schoot, A. P. H. J. Schenning, and E. W. Meijer, *Science*, 2006, **313**, 80–83.

S3. R. Kudo, R. Kawai, S. Takamiya, S. Datta, H. Hanayama, N. Hara, H. Tamiaki, and S. Yagai, *Chem. Commun.,* 2025, **61**, 8427–8430.

S4. T. Fukushima, K. Tamaki, A. Isobe, T. Hirose, N. Shimizu, H. Takagi, R. Haruki, S. Adachi, M. J. Hollamby, and S. Yagai, *J. Am. Chem. Soc.*, 2021, **143**, 5845–5854.